IIETA International Information and Engineering Technology Association
Advancing the World of Information and Engineering

Journal Européen des Systèmes Automatisés
Vol. 59, No. 1, January, 2026, pp. 285-292
Journal homepage: http://iieta.org/journals/jesa

Accurate Modeling and Optimization of Stator Core Loss in Permanent Magnet Synchronous Motors

Ran Zhou[1], Keqilao Meng[2*], Rihan Hai[2]

[1] College of Energy and Power Engineering, Inner Mongolia University of Technology, Hohhot 015000, China
[2] School of Renewable Energy, Inner Mongolia University of Technology, Ordos 017010, China

Corresponding Author Email: mengkeqilao23@163.com

https://doi.org/10.18280/jesa.590125

Received: 10 November 2025
Revised: 13 January 2026
Accepted: 22 January 2026
Available online: 31 January 2026

Keywords:
permanent magnet synchronous motor, stator core-loss modeling, Kriging surrogate model, Latin hypercube sampling, multi-objective optimization algorithm, optimization design

ABSTRACT

Permanent magnet synchronous motors are widely employed in new energy systems, industrial drives, and electric transportation, where increasingly stringent requirements are imposed on efficiency and loss control. However, under non-sinusoidal current and magnetic field conditions, stator core loss (also known as iron loss) exhibits highly nonlinear characteristics. Conventional core-loss models based on steady-state or sinusoidal assumptions are therefore unable to accurately represent actual losses, which limits the effectiveness of design optimization. In this study, an accurate stator core-loss model was established based on time-domain magnetic field decomposition. A Kriging surrogate model constructed using Latin hypercube sampling was integrated with a controlled elitist non-dominated sorting multi-objective genetic algorithm for global optimization. The optimization results indicate that stator core loss was reduced by 117.55 W, corresponding to a 47.6% decrease, while constraints on output power and efficiency were simultaneously satisfied. These results demonstrate that the proposed modeling and optimization framework provides an effective and reliable approach for addressing complex nonlinear electromagnetic optimization problems in permanent magnet synchronous motor design.

1. INTRODUCTION

With the rapid deployment of high-performance permanent magnet synchronous motors in new energy systems, industrial drive systems, and electric transportation, increasingly stringent requirements have been imposed on motor efficiency and loss reduction [1-3]. Consequently, higher levels of accuracy and computational efficiency are required in motor performance evaluation and design optimization. In conventional practice, the Bertotti frequency-domain core-loss model is commonly adopted to estimate motor core loss and to support performance analysis and optimization [3]. However, under practical operating conditions, permanent magnet synchronous motors are often subjected to non-sinusoidal current excitation and magnetic field waveforms. As a result, stator core loss exhibits pronounced nonlinear characteristics, and conventional core-loss models based on steady-state or purely sinusoidal assumptions are unable to accurately represent the actual loss behavior [4-8].

Meanwhile, permanent magnet synchronous motor design involves a large number of structural parameters that exhibit strong nonlinear coupling relationships. Traditional optimization approaches therefore tend to become trapped in local Pareto-optimal solutions, which limits the ability to achieve coordinated multi-objective optimization [9-13]. At present, the surrogate model–assisted Non-dominated Sorting Genetic Algorithm II is widely employed for multi-objective optimization of electromagnetic devices. However, during the environmental selection stage, a strict absolute elitism preservation strategy is typically adopted. When applied to complex solution spaces containing substantial subharmonic and harmonic electromagnetic components, this mechanism can easily lead to the loss of lateral population diversity, causing the algorithm to become trapped in local Pareto-optimal regions during the later stages of the search [14-16].

To address the aforementioned challenges, an accurate stator core-loss modeling approach based on time-domain magnetic field decomposition was developed. The proposed framework was further integrated with a Kriging surrogate model and a controlled elitist non-dominated sorting multi-objective genetic algorithm to enable efficient global optimization. Through this approach, stator core loss under non-sinusoidal magnetic field conditions was accurately characterized, while optimal design of structural parameters was simultaneously achieved under constraints on output power and efficiency. Optimization results demonstrate that the proposed framework provided significant advantages in reducing stator core loss and improving overall motor performance. These findings further confirmed the effectiveness and robustness of the proposed methodology for complex nonlinear electromagnetic optimization problems in permanent magnet synchronous motor design.

2. ACCURATE CORE-LOSS MODELING

2.1 Classical frequency-domain core-loss model

The widely adopted Bertotti frequency-domain core-loss model was originally proposed in 1988. Based on the physical mechanisms responsible for core-loss generation, the total core loss P_{Fe} can be decomposed into three components when the magnetic flux density waveform is assumed to be sinusoidal:

$$P_{Fe} = P_h + P_c + P_e = k_h f B_m^{\alpha} + k_c f^2 B_m^2 + k_e f^{1.5} B_m^{1.5} \tag{1}$$

where, P_h represents hysteresis loss, P_c denotes eddy current loss, and P_e corresponds to excess loss, α is an empirical coefficient, B_m denotes the amplitude of the magnetic flux density, k_h is the hysteresis-loss coefficient, k_c is the eddy-current-loss coefficient, and k_e is the excess-loss coefficient. Through analysis of the Bertotti core-loss separation model, it can be observed that accurate estimation of core loss can be achieved under sinusoidal, low-frequency unsaturated magnetic fields. However, when the magnetic field becomes non-sinusoidal, significant deviations may arise between the calculated and actual core-loss values [17-19].

2.2 Accurate core-loss modeling under non-sinusoidal magnetic fields

Analysis of the Bertotti core-loss separation model indicates that the formulation in Eq. (1) is derived under the assumption that the magnetic flux density waveform is sinusoidal. However, in practical electrical machines, the magnetic flux density in the air gap and the induced flux within the stator core are rarely purely sinusoidal. This behavior arises from factors such as the magnetization direction of permanent magnets and slotting effects. Consequently, the resulting magnetic field contains significant harmonic components. When core loss is evaluated using a time-domain approach, the instantaneous waveform of the induced magnetic field can be directly processed without decomposing it into a sinusoidal fundamental component and its harmonic components. This strategy eliminates errors introduced by harmonic approximation or truncation, thereby enabling more accurate characterization of stator core loss under non-sinusoidal excitation conditions.

To accurately quantify core loss under complex magnetic field conditions, the magnetic flux density vector $B(t)$ at an arbitrary spatial position is decomposed into radial and tangential components, denoted as $B_r(t)$ and $B_\theta(t)$, respectively, within an orthogonal coordinate system. Assuming that the magnetic material exhibits isotropic properties, the total core loss can be expressed as the nonlinear superposition of losses generated by alternating magnetic fields along the two orthogonal directions.

Hysteresis loss arises from the continuous reorientation of magnetic domains in ferromagnetic materials under an alternating magnetic field, which results in irreversible energy dissipation. The rainflow counting method is employed to evaluate the hysteresis loops generated by the fundamental magnetic field component, allowing the reconstruction of hysteresis loss. Accordingly, the hysteresis-loss formulation is modified as follows [20]:

$$P_h = \frac{k_h}{T}\left(\sum_{i=1}^{N_r}|\Delta B_{r,i}|^{\alpha} + \sum_{j=1}^{N_\theta}|\Delta B_{\theta,j}|^{\alpha}\right) \tag{2}$$

where, N_r and N_θ denote the effective numbers of local hysteresis loops extracted from the radial and tangential magnetic flux density components, respectively.

The time-domain integral expressions for classical eddy-current loss and excess loss can be derived based on the law of electromagnetic induction and statistical loss theory. According to these principles, classical eddy-current loss is proportional to the square of the rate of change of magnetic flux density, whereas excess loss is proportional to the 1.5 power of the rate of change of magnetic flux density. By substituting the orthogonally decomposed magnetic flux density components into the time-domain integral formulation, the expressions below can be obtained.

The time-domain classical eddy-current loss P_c is given by:

$$P_c = \frac{k_c}{2\pi^2 T}\int_0^T\left[\left(\frac{dB_r(t)}{dt}\right)^2 + \left(\frac{dB_\theta(t)}{dt}\right)^2\right]dt \tag{3}$$

The time-domain excess loss P_e is expressed as:

$$P_e = \frac{k_e}{8.76T}\int_0^T\left[\left|\frac{dB_r(t)}{dt}\right|^{1.5} + \left|\frac{dB_\theta(t)}{dt}\right|^{1.5}\right]dt \tag{4}$$

Accordingly, the accurate time-domain stator core-loss model under non-sinusoidal magnetic field conditions can be expressed as follows:

$$\begin{aligned} P_{Fe} &= P_h + P_c + P_e \\ &= \frac{k_h}{T}\left(\sum_{i=1}^{N_r}|\Delta B_{r,i}|^{\alpha} + \sum_{j=1}^{N_\theta}|\Delta B_{\theta,j}|^{\alpha}\right) \\ &\quad + \frac{k_c}{2\pi^2 T}\int_0^T\left[\left(\frac{dB_r(t)}{dt}\right)^2 + \left(\frac{dB_\theta(t)}{dt}\right)^2\right]dt \\ &\quad + \frac{k_e}{8.76T}\int_0^T\left[\left|\frac{dB_r(t)}{dt}\right|^{1.5} + \left|\frac{dB_\theta(t)}{dt}\right|^{1.5}\right]dt \end{aligned} \tag{5}$$

Based on the preceding calculations, it can be observed that the suppression of high-order harmonic components responsible for increased hysteresis loss is essential. At the same time, the distribution of leakage magnetic flux and the saturation level near the stator tooth tips must be regulated in order to further mitigate harmonic distortion. Under these considerations, the optimization of key structural parameters—including the permanent magnet pole arc coefficient, air-gap length, slot opening width, and permanent magnet thickness—is identified as an effective approach. Accordingly, a sensitivity analysis was conducted for the above parameters. Subsequently, multi-objective optimization was performed by taking stator core loss and motor performance indicators, including efficiency and output torque, as the objective functions.

3. SENSITIVITY ANALYSIS OF CORE-LOSS INFLUENCING PARAMETERS

3.1 Optimized motor configuration

A 10 kW permanent magnet direct-drive synchronous generator with 48 pole pairs and 87 stator slots was selected as the research object. The rotor magnetic circuit adopts a surface-mounted permanent magnet structure. The principal design parameters of the machine are summarized in Table 1.

Table 1. Main parameters of the investigated machine

Parameter	Value	Unit	Parameter	Value	Unit
Rated power	10	kW	Air-gap length	2.5	mm
Rated speed	120	rpm	Slot opening width	3	mm
Number of pole pairs	48	-	Slot depth	47.1	mm
Number of stator slots	87	-	Pole-arc coefficient	0.86	-
Permanent magnet thickness	7	mm			

3.2 Sensitivity analysis of design parameters

A finite element parametric sweep was performed to evaluate the sensitivity of the selected design parameters and to determine their corresponding optimization effectiveness and feasible design boundaries. The sweep range was defined by taking the initial electromagnetic design obtained from the magnetic circuit calculation as the central reference point, with the parameter values gradually expanded toward both upper and lower limits. During the analysis, each design parameter was varied independently, while all remaining parameters were kept constant. The results are illustrated in Figure 1.

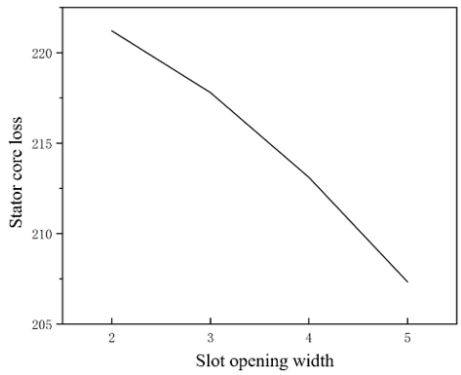

(a) Variation of stator core loss with slot opening width

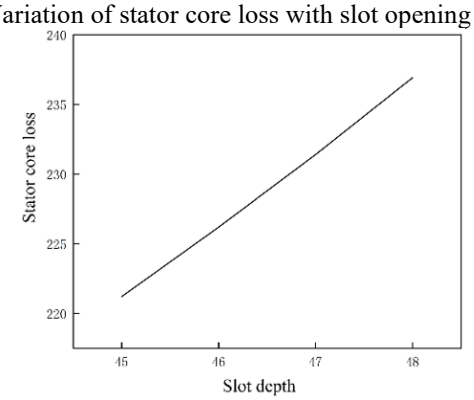

(b) Variation of stator core loss with slot depth

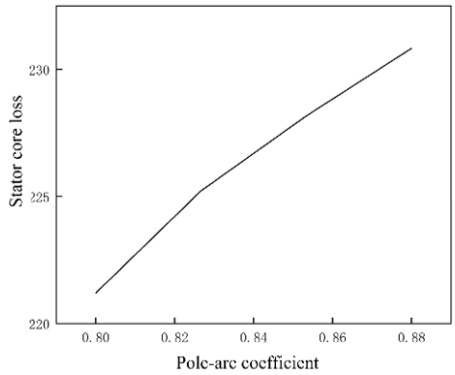

(c) Variation of stator core loss with pole-arc coefficient

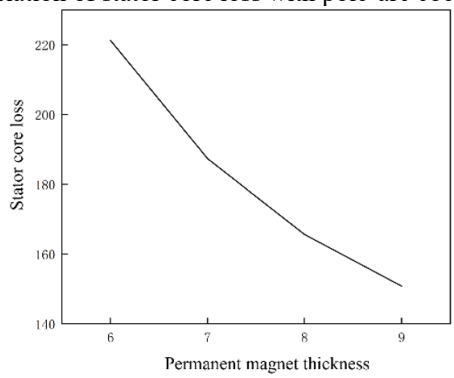

(d) Variation of stator core loss with permanent magnet thickness

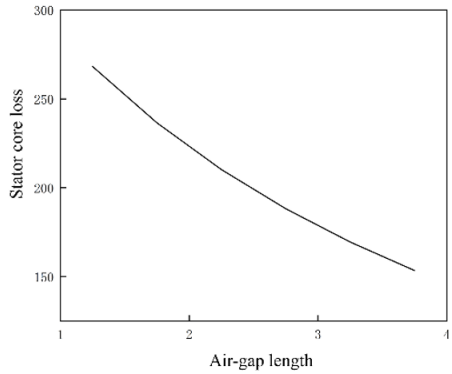

(e) Variation of stator core loss with air-gap length

Figure 1. Variation curves of stator core loss with respect to key motor parameters

As illustrated in Figure 1, stator core loss varies with changes in the five parameters. However, the degree of influence exerted by each parameter on stator core loss is different. In addition to reducing stator core loss, it is essential to ensure that the electromagnetic performance of the motor remains optimized during the design process. Therefore, efficiency and output torque were selected as additional performance indicators for evaluation. Parametric sweep calculations were further conducted for each design variable. The sensitivity of each parameter was then quantified. The sensitivity calculation was performed using the formulation given in Eq. (6), and the resulting sensitivity distributions are presented in Figure 2.

$$S_{Ai} = \left| \frac{\left[f(x_0 \pm \Delta x_i) - f(x_0) \right] / f(x_0)}{\pm \Delta x_i / x_0} \right| \tag{6}$$

where, S_{Ai} denotes the sensitivity of each parameter. By summing the calculated sensitivity values, it is observed that

the slot opening width exhibits relatively low sensitivity. Consequently, the permanent magnet pole-arc coefficient, slot depth, air-gap length, and permanent magnet thickness were selected as the primary design variables for subsequent optimization.

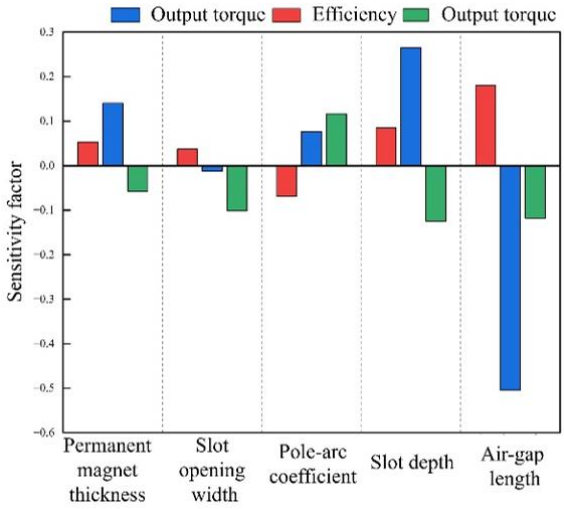

Figure 2. Sensitivity analysis of key parameters

4. OPTIMIZATION OF STATOR CORE LOSS

Currently, optimization approaches for improving motor performance can generally be classified into two categories. The first category consists of analytical optimization methods, whereas the second category involves design-of-experiments-based optimization methods. Optimization methods based on experimental design can be further divided into three main types: the Taguchi method, direct optimization based on intelligent algorithms, and surrogate model–based optimization methods. Among these approaches, surrogate model–based optimization has high computational efficiency and strong predictive capability. The fundamental principle of surrogate model–based optimization is to construct a model that describes the relationship between input design parameters and output performance indicators using a limited number of finite element simulation samples. This approach can provide a basis for subsequent optimization of additional motor performance indicators. In this study, a surrogate model–based optimization framework was employed to minimize stator core loss in the permanent magnet synchronous motor, thereby improving the overall electromagnetic performance of the machine.

4.1 Finite element sampling

Prior to constructing the surrogate model, samples must first be generated within the design space defined by the optimization ranges of the selected parameters, and corresponding finite element simulations must be performed. This process is commonly referred to as sampling. The selection of the sampling strategy has a significant influence on the result of the generated sample set. In this study, the Latin hypercube sampling method was adopted. Latin hypercube sampling, also known as stratified random sampling, allows the global distribution of design variables to be effectively represented using a relatively small number of samples. Consequently, the sampling efficiency of the optimization process can be significantly improved. The sampled design parameters include the pole-arc coefficient, air-gap length, slot depth, and permanent magnet thickness. The generated sample data are summarized in Table 2.

Table 2. Sample data

Sample	Permanent Magnet Thickness (mm)	Pole-Arc Coefficient	Slot Depth (mm)	Air-Gap Length (mm)
Sample 1	7.0	0.84	42.95	2.92
Sample 2	7.2	0.89	48.60	2.84
Sample 3	6.3	0.86	50.11	2.36
…	…	…	…	…
Sample *n*	7.11	0.93	47.47	2.76

4.2 Surrogate model comparison

The Kriging model exhibits high prediction accuracy and computational efficiency. In addition, it is well suited for addressing complex nonlinear optimization problems, such as those encountered in electromagnetic design of electrical machines. Compared with artificial intelligence–based models such as neural networks, the Kriging model requires significantly fewer training samples. The Kriging surrogate model can be expressed as:

$$y(x) = f(x) + z(x) \tag{7}$$

where, x denotes the design parameter, $y(x)$ represents the approximated response function, $f(x)$ represents the global approximation model of the polynomial response surface, and $z(x)$ corresponds to the local deviation term.

In Eq. (7), the term $z(x)$ is modeled as a stationary Gaussian random process with a mean value of zero and covariance σ^2.

$$\mathrm{cov}[z(x_i), z(x_j)] = \sigma^2 R[R(x_i, x_j)] \tag{8}$$

where, $R[]$ denotes the correlation matrix, and $R(x_i,x_j)$ represents the correlation function between two sample points. The Gaussian correlation function of $R(x_i,x_j)$ can be written as:

$$R(x_i, x_j) = \exp(-\sum_{k=1}^{m} \theta_k \mid x_{ik} - x_{jk} \mid) \tag{9}$$

where, m denotes the number of design variables, and θ_k represents the unknown correlation coefficient of the approximated surrogate model. The estimated value of $y(x)$ at the point x can be expressed as follows:

$$\hat{y} = \hat{\beta} + r^T(x) R^{-1}(y - f\hat{\beta}) \tag{10}$$

where, y denotes an n-dimensional unit column vector, and r^T represents the correlation vector.

$$\begin{aligned} r(x) &= [R(x, x_1), R(x, x_2) \cdots R(x, x_n)] \\ \hat{\beta} &= (f^T R^{-1} f)^{-1} f^T R^{-1} y \end{aligned} \tag{11}$$

The variance estimation can be written as:

$$\hat{\sigma}^2 = \frac{(y - f\hat{\beta})^T R^{-1} (y - f\hat{\beta})}{n} \tag{12}$$

The maximum likelihood estimation for fitting the Kriging model can be expressed as:

$$\max \Phi(\theta_k) = \frac{n \ln(\hat{\sigma}^2) + \ln |R|}{2} \tag{13}$$

By solving the k-dimensional nonlinear optimization problem, the Kriging model can be obtained (Figure 3).

Figure 3 presents the three-dimensional Kriging surrogate model relationships between stator core loss and the optimized structural parameters.

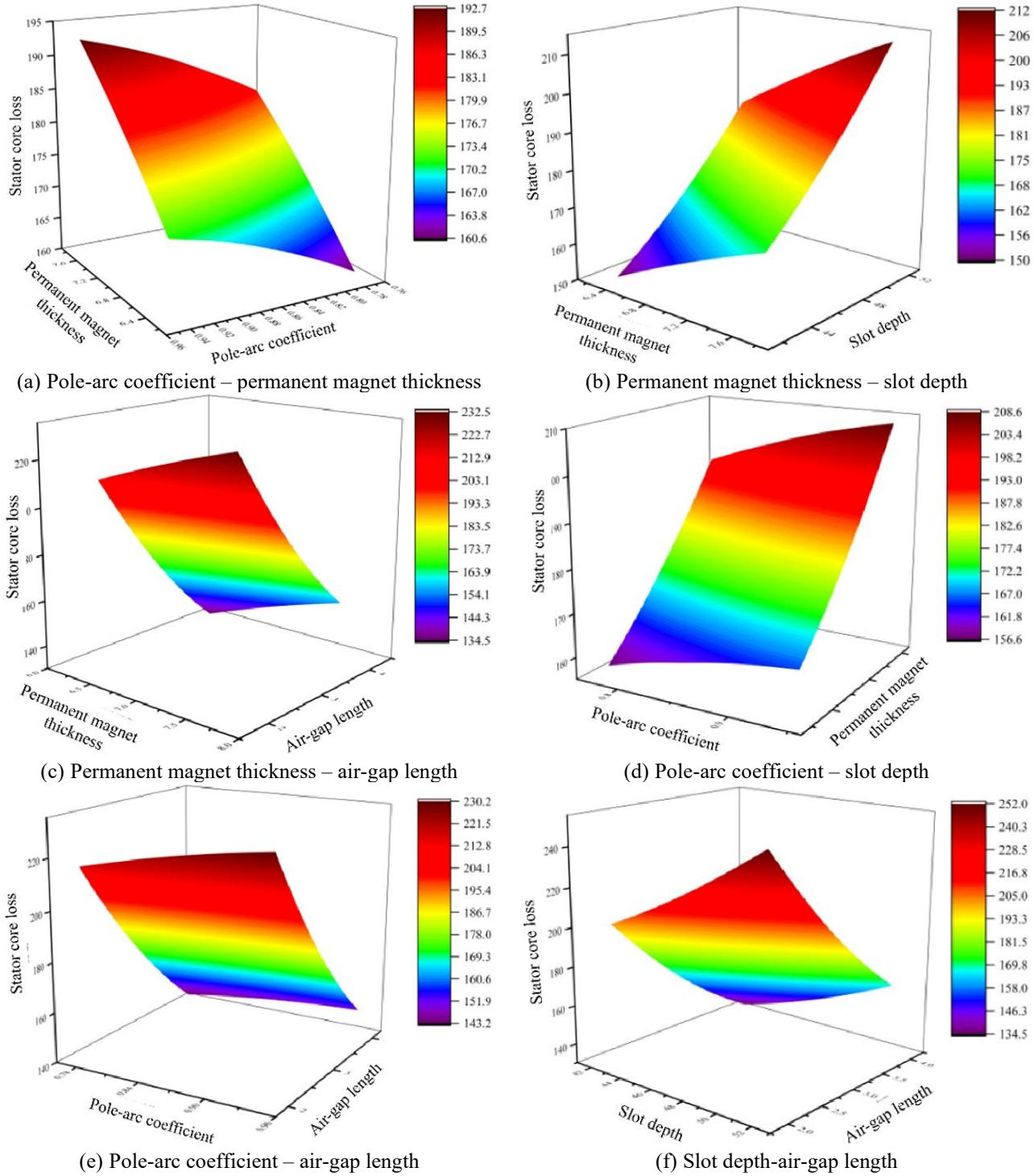

(a) Pole-arc coefficient – permanent magnet thickness

(b) Permanent magnet thickness – slot depth

(c) Permanent magnet thickness – air-gap length

(d) Pole-arc coefficient – slot depth

(e) Pole-arc coefficient – air-gap length

(f) Slot depth-air-gap length

Figure 3. Kriging surrogate model of stator core loss

4.3 Model validation

The input parameters of the sampled dataset consisted of the pole-arc coefficient, air-gap length, slot depth, and permanent magnet thickness, while the output parameters included the stator core loss under no-load conditions, as well as the output power and efficiency under generator operating conditions. The Kriging surrogate model constructed using Latin hypercube sampling was trained with 300 sample points. The resulting model was capable of accurately capturing both the global and local characteristics of the relationship between the input design variables and the output performance indicators. To evaluate the predictive accuracy of the surrogate model, the coefficient of determination (R^2) was employed as the

validation metric:

$$R^2 = 1 - \frac{\sum_{i=1}^{N}(y - \hat{y}_i)}{\sum_{i=1}^{N}(y_i - \bar{y}_i)} \tag{14}$$

where, N denotes the number of testing points, y_i represents the actual value of the i-th testing point, $\hat{y}_i$ denotes the predicted value of the i-th testing point, and $\bar{y}_i$ represents the mean value of the observed data for N testing points. A value of R^2 closer to 1 indicates higher predictive accuracy of the surrogate model. The calculated prediction coefficients are presented in Figure 4, which demonstrates that the constructed surrogate model achieves a high degree of fitting accuracy.

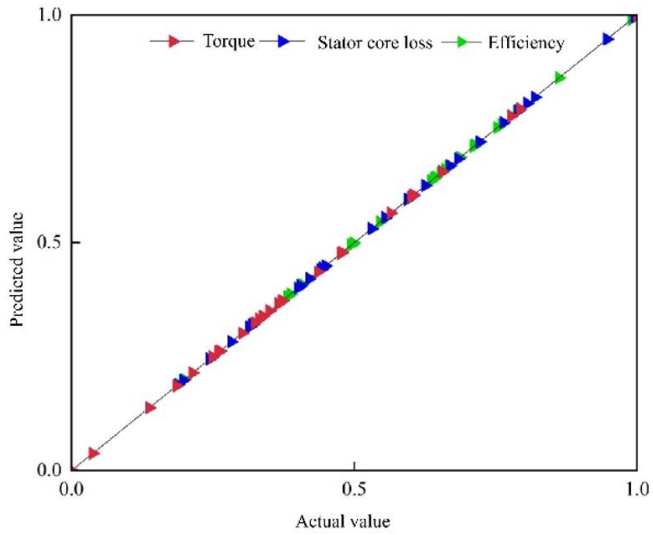

Figure 4. Prediction accuracy of the Kriging surrogate model for stator core loss (the coefficient of determination R^2)

The calculated coefficient of determination for the Kriging surrogate model of stator core loss is 0.98, indicating that the constructed surrogate model achieves high prediction accuracy.

4.4 Surrogate model–Assisted optimization

In the multidimensional parameter optimization of permanent magnet synchronous generators, conventional heuristic optimization algorithms are prone to becoming trapped in local Pareto-optimal regions during the later stages of the search process. To address this limitation, a non-dominated sorting multi-objective genetic algorithm based on the controlled elitism strategy (controlled-elitism Non-dominated Sorting Genetic Algorithm II, a multi-objective genetic algorithm) was adopted to perform global optimization.

In the traditional Non-dominated Sorting Genetic Algorithm II algorithm, environmental selection is performed strictly according to the non-dominated sorting rank of the Pareto fronts (Front i) and the crowding distance. When the number of non-dominated individuals in the first front (Front 1) exceeds the predefined population size N, individuals belonging to inferior fronts (Front 2, Front 3, …) are completely excluded by the algorithm. To maintain the spatial exploration capability of the population, the multi-objective genetic algorithm introduces a controlled elitism strategy, in which the number of individuals allowed to enter the next generation from each Pareto front is strictly constrained according to a geometrically decreasing distribution.

Assuming that the population size is N and the current population is divided into K non-dominated fronts, the controlled elitism strategy specifies that the maximum number of individuals allowed to enter the next generation from the i-th front, denoted as n_i, follows the geometric sequence:

$$n_i = r \cdot n_{i-1} \tag{15}$$

where, r represents the hierarchical decay coefficient, with $r<1$. Meanwhile, the total number of individuals retained from all Pareto fronts must satisfy the population size constraint, which can be expressed as:

$$\sum_{i=1}^{K} n_i = N \tag{16}$$

By jointly solving the above equations, the retention quotas for each Pareto front level, ranging from the globally optimal solutions to relatively inferior solutions, can be determined with precision. The Pareto solution set obtained for stator core loss using the multi-objective genetic algorithm is illustrated in Figure 5.

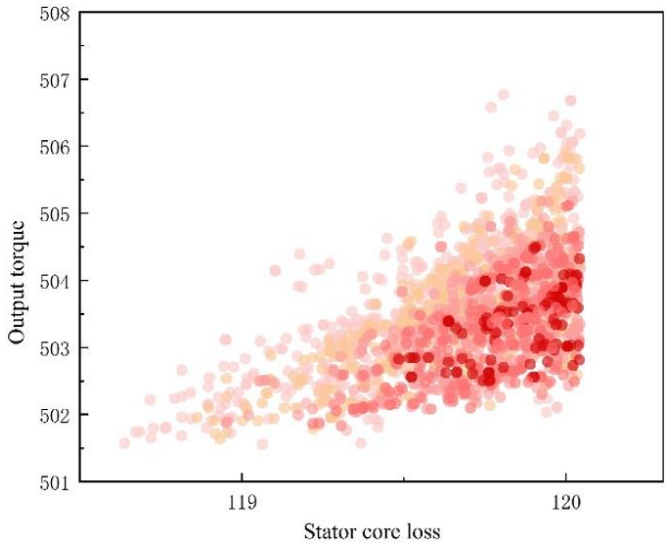

Figure 5. Pareto solution set of stator core loss and output torque for the motor

Based on the obtained Pareto solution set, the final optimized parameters can be selected and are summarized in Table 3.

Table 3. Optimal design parameters

Parameter	Value
Permanent magnet thickness (mm)	6.3
Pole-arc coefficient	0.77
Slot depth (mm)	42.4
Air-gap length (mm)	3.8

To verify the effectiveness of the optimization strategy, the optimized parameters were applied to the motor model and evaluated. The results were then compared with those of the initial design, as summarized in Table 4. The results indicate that, after optimization, stator core loss is reduced by 117.55 W, corresponding to a reduction of 47.6%. Meanwhile, the

motor efficiency increases from 92.4% to 95.6%. The output torque decreases slightly from 506.88 N·m to 501.58 N·m, which does not significantly affect the overall output performance of the motor.

Table 4. Performance comparison between the initial design and the optimized design

Performance Indicator	Initial Design	Optimized Design
Stator core loss (W)	226.19	118.64
Output torque (N·m)	506.88	501.58
Efficiency (%)	92.4	95.6

5. CONCLUSION

A time-domain stator core-loss model based on magnetic field decomposition was introduced to accurately characterize core loss under non-sinusoidal magnetic field conditions. Based on the proposed model, several key motor design parameters closely related to stator core loss were identified. A Kriging surrogate model constructed using Latin hypercube sampling was subsequently developed, and a controlled-elitist non-dominated sorting multi-objective genetic algorithm was employed to achieve efficient global optimization. The results demonstrate that the constructed Kriging surrogate model exhibits high predictive accuracy, and its integration with the multi-objective genetic algorithm effectively can overcome the tendency of conventional optimization methods to become trapped in local Pareto-optimal solutions. Under the constraints of output power and efficiency, the optimized motor structure reduced stator core loss by 117.55 W, corresponding to a reduction of 47.6%, while significantly improving overall motor performance. These results confirm that the proposed stator core-loss model and optimization strategy provide an effective and reliable approach for addressing complex nonlinear electromagnetic optimization problems in permanent magnet synchronous machine design.

REFERENCES

[1] Zhu, Y., Liu, Z.M., Zhao, W.X., et al. (2025). Overview of iron loss calculation methods for flux modulation electric machines. Proceedings of the CSEE, 45(13): 5294-5307. https://doi.org/10.13334/j.0258-8013.pcsee.241588

[2] Kong, X.G., Wang, F.X., Xu, Y.L., et al. (2010). Analysis and calculation of iron loss in high-speed permanent magnet motors. Electric Machines and Control, 14(9): 5. https://doi.org/10.3969/j.issn.1007-449X.2010.09.005

[3] Tong, W.M., Sun, J.Y., Duan, Q. L., et al. (2017). Study on no-load iron loss of permanent magnet synchronous motors. Electric Machines and Control, 21(5): 51-57. https://doi.org/10.15938/j.emc.2017.05.007

[4] Chen, B., Cai, W.J., Feng, Y. Z., et al. (2024). Simulation method for dynamic hysteresis characteristics of high-frequency transformer cores under non-sinusoidal excitation. Proceedings of the CSEE, 44(13): 5420-5430. https://doi.org/10.13334/j.0258-8013.pcsee.230386

[5] Chai, F., Liang, P., Pei, Y., Cheng, S. (2016). Magnet shape optimization of surface-mounted permanent-magnet motors to reduce harmonic iron losses. IEEE Transactions on Magnetics, 52(7): 1-4. https://doi.org/10.1109/TMAG.2016.2524010

[6] Tian, Z., Zhang, C., Zhang, S. (2017). Analytical calculation of magnetic field distribution and stator iron losses for surface-mounted permanent magnet synchronous machines. Energies, 10(3): 320. https://doi.org/10.3390/en10030320

[7] Zhang, X., Fu, P., Ma, Y., Zhang, C., Li, L. (2018). No-load iron loss model for a fractional-slot surface-mounted permanent magnet motor based on magnetic field analytical calculation. Chinese Journal of Electrical Engineering, 4(4): 71-79. https://doi.org/10.23919/CJEE.2018.8606792

[8] Yu, Z., Li, Y., Jing, Y., Du, J., Wang, Z. (2020). Analytical model for magnetic field calculation of SPMSM with chamfered pole considering iron core saturation. IET Electric Power Applications, 14(10): 1856-1864. https://doi.org/10.1049/iet-epa.2019.1013

[9] Wu, S., Huang, X., Tian, C., Zhang, P. (2019). Multi-physical field optimization analysis of high-speed permanent magnet synchronous motor based on NSGA-II algorithm. In 2019 22nd International Conference on Electrical Machines and Systems (ICEMS), Harbin, China, pp. 1-6. https://doi.org/10.1109/ICEMS.2019.8922236

[10] Shen, N., Li, D., Stork, W. (2020). 3-D shape optimization of a sensor mounting arm using MOGA and MLF. In 2020 12th International Conference on Advanced Computational Intelligence (ICACI), Dali, China, pp. 602-608. https://doi.org/10.1109/ICACI49185.2020.9177734

[11] Tong, J., Wang, Y., Liu, X.W., Li, X.F., Wei, Y., Kouh, J.S. (2018). Parametric design and deformation optimization of series propellers based on MOGA and CFD. In 2018 OCEANS-MTS/IEEE Kobe Techno-Oceans (OTO), Kobe, Japan, pp. 1-7. https://doi.org/10.1109/OCEANSKOBE.2018.8559044

[12] Bertotti, G. (1988). General properties of power losses in soft ferromagnetic materials. IEEE Transactions on Magnetics, 24(1): 621-630. https://doi.org/10.1109/20.43994

[13] Zhu, J.G., Ramsden, V.S. (1998). Improved formulations for rotational core losses in rotating electrical machines. IEEE Transactions on Magnetics, 34(4): 2234-2242. https://doi.org/10.1109/20.703861

[14] Eggers, D., Steentjes, S., Hameyer, K. (2012). Advanced iron-loss estimation for nonlinear material behavior. IEEE Transactions on Magnetics, 48(11): 3021-3024. https://doi.org/10.1109/TMAG.2012.2208944

[15] Xu, K., Guo, Y., Lei, G., Zhu, J. (2023). Estimation of iron loss in permanent magnet synchronous motors based on particle swarm optimization and a recurrent neural network. Magnetism, 3(4): 327-342. https://doi.org/10.3390/magnetism3040025

[16] Asef, P., Bargallo, R., Lapthorn, A.C. (2019). Time-domain computation of rotational iron losses considering the bulk conductivity for PMSMs. IET Electric Power Applications, 13(6): 776-785. https://doi.org/10.1049/iet-epa.2018.5395

[17] Diao, C., Zhao, W., Li, L., Kwon, B.I. (2024). Optimization design of surface permanent magnet synchronous motor with hybrid magnets using analytical method. In 2024 IEEE 21st Biennial Conference on Electromagnetic Field Computation (CEFC), Jeju, Korea,

Republic of, pp. 1-2. https://doi.org/10.1109/CEFC61729.2024.10586134
[18] Diao, C., Zhao, W., Li, L., Liu, C., Tian, M., Wang, X. (2024). Analytical modeling and optimization of permanent magnet synchronous machine with hybrid magnets. IEEE Transactions on Industry Applications, 61(1): 243-254. https://doi.org/10.1109/TIA.2024.3481390
[19] Du, G., Xu, W., Zhu, J., Huang, N. (2019). Effects of design parameters on the multiphysics performance of high-speed permanent magnet machines. IEEE Transactions on Industrial Electronics, 67(5): 3472-3483. https://doi.org/10.1109/TIE.2019.2922933
[20] Boglietti, A., Cavagnino, A., Lazzari, M., Pastorelli, M. (2003). Predicting iron losses in soft magnetic materials with arbitrary voltage supply: An engineering approach. IEEE Transactions on Magnetics, 39(2): 981-989. https://doi.org/10.1109/TMAG.2003.808599